REFERENCES

Alonso L, Fuchs E (2006) The hair cycle. *J Cell Sci* 119:391–3

Jindo T, Imai R, Takamori K, Ogawa H (1993) Organ culture of mouse vibrissal hair follicles in serum-free medium. *J Dermatol* 20:756–62

Nakamura M, Sundberg JP, Paus R (2001) Mutant laboratory mice with abnormalities in hair follicle morphogenesis, cycling, and/or structure: annotated tables. *Exp Dermatol* 10:369–90

Oshima H, Rochat A, Kedzia C, Kobayashi K, Barrandon Y (2001) Morphogenesis and renewal of hair follicles from adult multipotent stem cells. *Cell* 104:233–45

Paus R, Cotsarelis G (1999) The biology of hair follicles. *New Engl J Med* 341:491–7

Philpott MP, Kealey T (2000) Cyclical changes in rat vibrissa follicles maintained *in vitro*. *J Invest Dermatol* 115:1152–5

Robinson M, Reynolds AJ, Jahoda CA (1997) Hair cycle stage of the mouse vibrissa follicle determines subsequent fiber growth and follicle behavior *in vitro*. *J Invest Dermatol* 108:495–500

Stenn KS, Paus R (2001) Controls of hair follicle cycling. *Physiol Rev* 81:449–94

Sundberg JP, Boggess D, Sundberg BA, Eilertsen K, Parimoo S, Filippi M *et al.* (2000) Asebia-2J (Scd1(ab2J)): a new allele and a model for scarring alopecia. *Am J Pathol* 156: 2067–75

Yano K, Brown LF, Detmar M (2001) Control of hair growth and follicle size by VEGF-mediated angiogenesis. *J Clin Invest* 107: 409–17

Young RD, Oliver RF (1976) Morphological changes associated with the growth cycle of vibrissal follicles in the rat. *J Embryol Exp Morphol* 36:597–607

The Importance of Long-Term Monitoring to Evaluate the Microvascular Response to Light-Based Therapies

Journal of Investigative Dermatology (2008) **128,** 485–488; doi:10.1038/sj.jid.5700991; published online 2 August 2007

TO THE EDITOR

Optimization of laser therapy for disfiguring vascular birthmarks is one specific clinical application (Kelly *et al.*, 2005). Current treatment protocols involve the use of high-power pulsed laser irradiation with parameters chosen to induce selective photocoagulation of the targeted blood vessels, a method known as selective photothermolysis (Anderson and Parrish, 1983). Protocol design is based largely on results from numerical modeling studies (van Gemert *et al.*, 1997), which are designed to predict the laser light distribution within the skin and subsequent photothermal response leading toward selective photocoagulation. However, current modeling methods do not incorporate adequately the complex dynamics associated with changes in light absorption due to conversion of hemoglobin to methemoglobin (Barton *et al.*, 2001; Kimel *et al.*, 2005) and convective mixing of blood during pulsed laser irradiation (Kimel *et al.*, 2003), limiting their overall predictive capability. Furthermore, these models do not consider the chronic, biological response of the microvasculature to therapeutic laser intervention, which remains a poorly researched field. Knowledge of the biological response is critical to understand the repair processes initiated with photothermal injury and to assess the ultimate efficacy of the treatment.

Animal models used as a platform to study light-based, microvascular-targeted therapies include the chick chorioallantoic membrane (Kimel *et al.*, 1994, 2003), hamster cheek pouch (Suthamjariya *et al.*, 2004), and rodent dorsal window chamber (Barton *et al.*, 1998, 1999, 2001; Choi *et al.*, 2004; Babilas *et al.*, 2005; Smith *et al.*, 2006). Optical imaging modalities used to evaluate noninvasively therapeutic outcome include video imaging, fluorescence microscopy, Doppler optical coherence tomography, and laser speckle imaging. Typically, short-term (<24 hours after intervention) evaluation of the microvasculature is performed. Babilas *et al.* (2005) proposed that a (1) 24-hour monitoring period allows for evaluation of ''delayed biological effects'' in the microvascular response to pulsed laser irradiation, and (2) the short-term response correlates well with numerical modeling predictions of photocoagulation. Longer (>24 hour after intervention) monitoring periods usually are not performed with nontumor-bearing window chambers, presumably due to the reduced clarity of the chamber imposed by poor maintenance of window integrity secondary to infection. However, we hypothesized that the short-term response of the microvasculature is a poor predictor of the long-term response. With emphasis on aseptic methods, we have been able to maintain clear window chamber preparations for as long as 45 days after intervention. With this model, we have studied the long-term microvascular response to light-based, microvascular-targeted therapies.

The data presented herein were acquired from adult male Golden Syrian hamsters. The surgery was performed as defined in a protocol approved by the University of California, Irvine, Animal Use Committee. The surgical protocol was a modified version of one described previously (Papenfuss *et al.*, 1979). For all steps, aseptic conditions were maintained. We used wide-field color reflectance imaging and laser speckle imaging (Choi *et al.*, 2004, 2006; Smith *et al.*, 2006) to document and evaluate quantitatively and chronically ensuing blood flow dynamics. In one set of experiments, we irradiated select arteriole-venule pairs with laser pulse sequences to evaluate the efficacy of various therapeutic protocols. In the presented example (Figure 1a), we irradiated an arteriole-venule pair (upper circle in ''Before'' image) with five laser pulses containing both 532 and 1064 nm laser wavelengths and a second pair (lower circle) with a single 532/1064 nm laser pulse. Numerical modeling data suggested that both sets of laser parameters should induce photocoagulation in the

targeted vessels (Dr Wangcun Jia, unpublished data). The short-term response was characterized primarily by photocoagulation events, with a substantial-to-complete venular flow reduction and considerable arteriolar flow reduction, a trend in agreement with data presented by Barton *et al.* (1999). At 24 hours after intervention, the arteriolar flow (circle in day 1 speckle flow index image) was absent.

At later time points, partial-to-complete restoration of blood flow in these photocoagulated vessels was observed (Figures 1a and b). In general, we observed several microvascular dynamics, including vasoconstriction, vasodilation, and delayed blood flow changes, in both directly irradiated and nonirradiated vessels. We have observed shunting of blood flow to tortuous collateral vessels (i.e., indicated by arrow in day 6 image). Furthermore, we have observed vessel repair within the same position as the original vessel (i.e., indicated by arrows in day 15 and day 21 images), suggesting that the vascular remodeling process may be associated with a ''memory'', in agreement with published tumor angiogenesis data (Mancuso *et al.*, 2006).

In a second set of experiments, we evaluated the efficacy of photodynamic therapy as a photochemical method to destroy the microvasculature. Two days after window chamber installation, we installed a jugular vein catheter for intravenous access, injected the photosensitizer benzoporphyrin monoacid ring

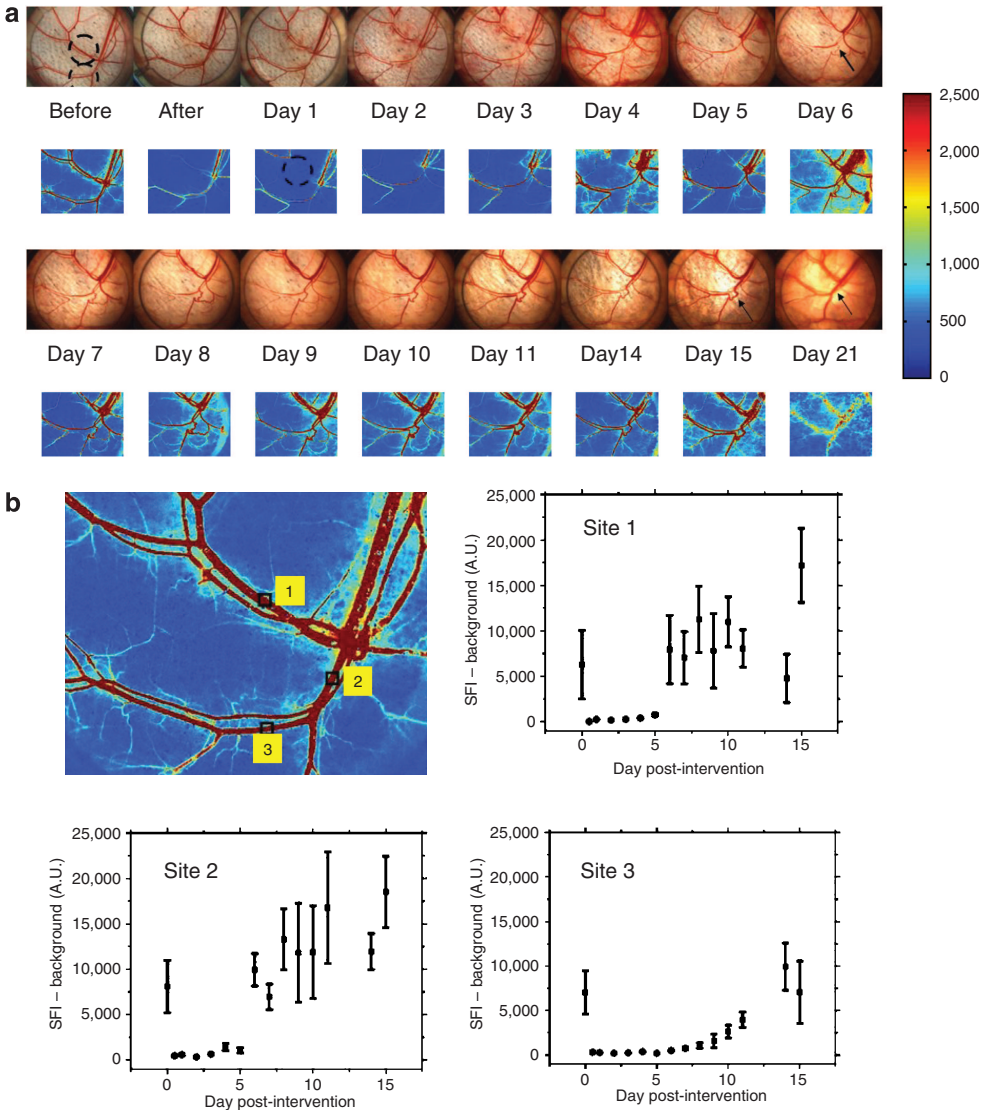

Figure 1. Microvascular blood flow response after pulsed laser irradiation. (**a**) Time sequence of wide-field color reflectance images (top row) and corresponding speckle flow index (SFI) images (bottom row) acquired over a 21-day monitoring period after pulsed laser irradiation of selected sites. Two arteriole-venule pairs (dashed circles in ''Before'' image) were irradiated with simultaneous 532 and 1064 nm laser pulses (upper circle—five 1-ms laser pulses at 27 Hz repetition rate, 2 J/cm^2 at 532 nm, 3.6 J/cm^2 at 1064 nm; lower circle—single 1-ms laser pulse, 4 J/cm^2 at 532 nm, 7.2 J/cm^2 at 1064 nm). Vascular remodeling and blood flow dynamics were evident during the 21-day monitoring period, with the day 0 and day 21 structural images having similar appearances. (**b**) Quantitative evaluation of selected blood vessel regions of interest. In all three regions, the blood flow was shut down immediately, followed by eventual reperfusion to near-baseline blood flow levels. Color reflectance image dimensions (H × V): 13 × 10 mm^2; SFI image dimensions: 9 × 7 mm^2.

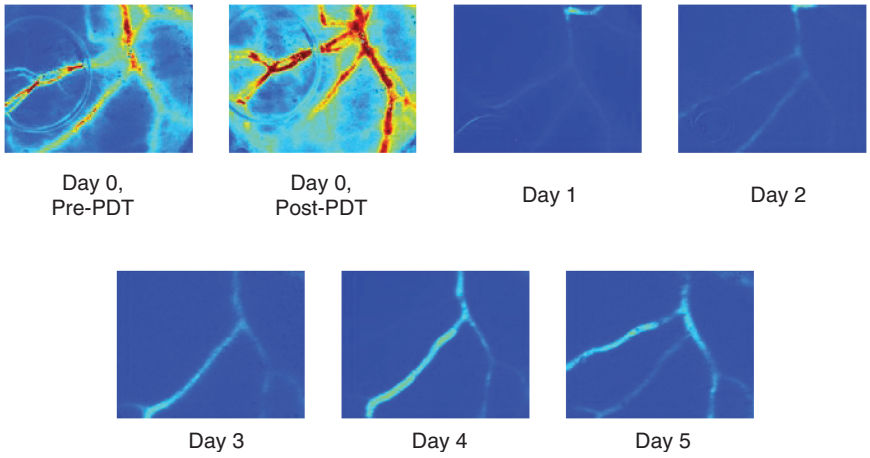

Figure 2. Microvascular blood flow response, assessed with laser speckle imaging, after photodynamic therapy. An ~4-mm diameter air bubble was present in the day 0 images, but it had no apparent effect on the speckle flow index (SFI) values. Benzoporphyrin monoacid ring A (1.5 mg/kg body mass) was administered via a jugular vein catheter. Fifteen minutes after benzoporphyrin monoacid ring A injection, continuous wave laser irradiation of the entire window chamber was performed with an argon-pumped dye laser (576 nm, 100 mW/cm^2 irradiance, 96 J/cm^2 radiant exposure). Irradiation was performed on the epidermal side of the chamber. A hyperemic response was observed immediately after photodynamic therapy, consistent with previous data (Smith *et al.*, 2006). At day 1, a large reduction in blood flow was observed, followed by a progressive increase in blood flow in the larger blood vessels. Image dimensions (H × V): 9 × 7 mm^2.

A, and used 576 nm laser light to excite the benzoporphyrin monoacid ring A. The experimental protocol was similar to the one we published previously (Smith *et al.*, 2006). At 24 hours post-photodynamic therapy, we have observed a considerable shutdown of the microcirculation in the entire window (Figure 2, day 1). However, starting at 3 days post-photodynamic therapy, we have observed a progressive, partial recovery of blood flow, illustrating once again the role of the biological response in mediating the ensuing hemodynamics.

Collectively, our data strongly suggest that the short-term (<24 hours) microvascular response to light-based therapeutic intervention differs considerably from the long-term response. We believe this is due to the biological repair response, which is not taken into account in current theoretical models. Such events have not been observed in previous studies on nontumor-bearing window chambers presumably due to tissue regrowth, which we have demonstrated can be minimized with maintenance of an aseptic surgical field. We have observed considerable vascular remodeling events and at least partial restoration of blood flow within initially photocoagulated blood vessels. Our animal model and optical imaging instrumentation allow us to perform chronic evaluation of novel therapeutic approaches designed to alter the microcirculation. Long-term evaluation is probably essential to provide meaningful data that can result ultimately in improved therapeutic outcome. For such evaluation, laser speckle imaging also can be used to perform ''image-guided microscopy'', to assess quantitatively the wide-field microvascular blood flow response to therapy. This information would be useful in judicious selection of specific regions of interest to probe further with higher resolution imaging modalities such as multiphoton microscopy or optical coherence tomography.

CONFLICT OF INTEREST

The authors state no conflict of interest.

ACKNOWLEDGMENTS

We thank Mr Thang Nguyen and Mr Dan Pattanachinda (School of Biological Sciences, University of California, Irvine) for their assistance. The work was funded in part by the American Cancer Society Institutional Research Grant (ACS-IRG 98-279-04, BC), Arnold and Mabel Beckman Foundation, and National Institutes of Health (AR051443 to KMK; and the Laser Microbeam and Medical Program (LAMMP), an NIH Biomedical Technology Resource, grant #P41-RR01192, at the University of California, Irvine).

Bernard Choi[1,2], Wangcun Jia[1], Jennifer Channual[1], Kristen M. Kelly[1,3] and Justin Lotfi[1]

[1]Beckman Laser Institute and Medical Clinic, University of California, Irvine, California, USA; [2]Department of Biomedical Engineering, University of California, Irvine, California, USA and [3]Department of Dermatology, University of California, Irvine, California, USA.
E-mail: choib@uci.edu

REFERENCES

Anderson RR, Parrish JA (1983) Selective photothermolysis—precise microsurgery by selective absorption of pulsed radiation. *Science* 220:524–7

Babilas P, Shafirstein G, Baumler W, Baier J, Landthaler M, Szeimies RM *et al.* (2005) Selective photothermolysis of blood vessels following flashlamp-pumped pulsed dye laser irradiation: *in vivo* results and mathematical modelling are in agreement. *J Invest Dermatol* 125:343–52

Barton JK, Frangineas G, Pummer H, Black JF (2001) Cooperative phenomena in two-pulse, two-color laser photocoagulation of cutaneous blood vessels. *Photochem Photobiol* 73:642–50

Barton JK, Vargas G, Pfefer TJ, Welch AJ (1999) Laser fluence for permanent damage of cutaneous blood vessels. *Photochem Photobiol* 70:916–20

Barton JK, Welch AJ, Izatt JA (1998) Investigating pulsed dye laser-blood vessel interaction with color Doppler optical coherence tomography. *Opt Express* 3:251–6

Choi B, Kang NM, Nelson JS (2004) Laser speckle imaging for monitoring blood flow dynamics in the *in vivo* rodent dorsal skin fold model. *Microvasc Res* 68:143–6

Choi B, Ramirez-San-Juan JC, Lotfi J, Nelson JS (2006) Linear response range characterization and *in vivo* application of laser speckle imaging of blood flow dynamics. *J Biomed Opt* 11:041129

Kelly KM, Choi B, McFarlane S, Motosue A, Jung BJ, Khan MH *et al.* (2005) Description and analysis of treatments for port-wine stain birthmarks. *Arch Facial Plast Surg* 7: 287–94

Kimel S, Choi B, Svaasand LO, Lotfi J, Viator JA, Nelson JS (2005) Influence of laser wavelength and pulse duration on gas bubble formation in blood filled glass capillaries. *Lasers Surg Med* 36:281–8

Kimel S, Svaasand LO, Hammerwilson M, Schell MJ, Milner TE, Nelson JS *et al.* (1994) Differential vascular-response to laser photothermolysis. *J Invest Dermatol* 103:693–700

Kimel S, Svaasand LO, Hammer-Wilson MJ, Nelson JS (2003) Influence of wavelength on response to laser photothermolysis of blood vessels: implications for port wine stain laser therapy. *Lasers Surg Med* 33:288–95

Mancuso MR, Davis R, Norberg SM, O'Brien S, Sennino B, Nakahara T *et al.* (2006) Rapid vascular regrowth in tumors after reversal of VEGF inhibition. *J Clin Invest* 116:2610–21

Papenfuss HD, Gross JF, Intaglietta M, Treese FA (1979) Transparent access chamber for the rat dorsal skin fold. *Microvasc Res* 18: 311–8

Smith TK, Choi B, Ramirez-San-Juan JC, Nelson JS, Osann K, Kelly KM (2006) Microvascular blood flow dynamics associated with photodynamic therapy, pulsed dye laser irradiation and combined regimens. *Lasers Surg Med* 38:532–9

Suthamjariya K, Farinelli WA, Koh W, Anderson RR (2004) Mechanisms of microvascular response to laser pulses. *J Invest Dermatol* 122:518–25

van Gemert MJC, Smithies DJ, Verkruysse W, Milner TE, Nelson JS (1997) Wavelengths for port wine stain laser treatment: influence of vessel radius and skin anatomy. *Phys Med Biol* 42:41–50

Absence of PDGFRA Mutations in Primary Melanoma

Journal of Investigative Dermatology (2008) **128,** 488–489; doi:10.1038/sj.jid.5701036; published online 30 August 2007

TO THE EDITOR

The mitogen-activated protein kinase signaling pathway plays an important role in cell proliferation, differentiation and survival and is frequently altered in cancer. Genetic mechanisms that activate the mitogen-activated protein-kinase pathway vary among subtypes of melanoma when tumors are classified according to a combination of sun exposure and anatomic site (Maldonado *et al.*, 2003; Curtin *et al.*, 2005, 2006). *NRAS* (neuroblastoma ras viral oncogene homolog), which is part of the RAS/RAF/mitogen-activated protein-kinase signaling cascade, is mutated in 10–20% of melanomas regardless of anatomic site. In contrast, v-raf murine sarcoma viral oncogene homolog B1 (*BRAF*) mutations are frequent (about 60%) in melanomas occurring on skin without signs of chronic sun-induced damage (CSD) (non-CSD melanomas), but infrequent in melanomas that occur on skin showing evidence of CSD as well as on sun-protected skin such as the palms, soles, or subungual sites (acral melanomas), and on mucosal membranes (mucosal melanomas) (Maldonado *et al.*, 2003; Curtin *et al.*, 2005). We have recently reported increased copy numbers of chromosome 4q12 and identified v-kit Hardy-Zuckerman 4 feline sarcoma viral oncogene homolog (*KIT*) as a somatic target that is activated in CSD, acral, and mucosal melanoma. This genomic region contains several additional genes that are involved in other types of cancer, including the platelet-derived growth factor α receptor (*PDGFRA*). *PDGFRA* is a receptor tyrosine kinase, which is activated by mutations or small deletions in a subset of gastrointestinal stroma tumors (Heinrich *et al.*, 2003b) and childhood acute myeloid leukaemia's (Hiwatari *et al.*, 2005) as well as fusion with *FIP1L1* in hypereosinophilic syndrome (Cools *et al.*, 2003) and systemic mastocytosis associated with eosinophilia (Pardanani *et al.*, 2003). Mutation of *PDGFRA* or *KIT* occurs infrequently in most solid tumors with the exception of gastrointestinal stroma tumors (Sihto *et al.*, 2005). In gastrointestinal stroma tumors, mutations in *PDGFRA* and *KIT* are mutually exclusive (Heinrich *et al.*, 2003a, b) and tumors with either mutation can show responses with kinase inhibitors such as imatinib, dasatinib, and sunitinib (Heinrich *et al.*, 2003a; Corless *et al.*, 2006; Schittenhelm *et al.*, 2006). PDGFRA has been found to be overexpressed in some melanomas (Barnhill *et al.*, 1996), raising the possibility that it could also be a target of somatic mutations in some melanomas. To date, a limited mutation analysis of primary tumors did not find mutations in *PDGFRA* (Curtin *et al.*, 2006). To address fully the role of *PDGFRA* in melanoma, we analyzed a larger set of primary melanomas for mutations, copy number increases, and expression of PDGFRA. To increase the likelihood of encountering mutations, we enriched the samples for cases that did not have mutations of *KIT* or *BRAF*.

Specifically, we analyzed DNA extracted from archival paraffin-embedded primary melanomas with an invasive component in which tumor cells predominated over stroma cells. Additional analyses on some of these cases were reported previously (Curtin *et al.*, 2005, 2006). Institutional Review Board of the University of California, San Francisco, approved the study. From a cohort of 102, we sequenced the 26 primary melanomas which had increased copy number of the 4q12 locus harboring *PDGFRA* ($n=10$) or had normal copy number but did not show mutations in *KIT* exons 11, 13, 17, and 18, and *BRAF* exon 15 ($n=16$). Seven of the cases were acral melanomas, that is melanomas from the palms, soles, and subungual sites; 13 were mucosal melanomas; and three were melanomas from chronically sun-damaged skin, and three melanoma from skin without chronic sun damage. CSD was defined by the microscopic presence or absence of marked solar elastosis of the dermis surrounding the melanomas. Exons of interest were amplified by PCR and sequenced as described previously (Curtin *et al.*, 2005) using specific primers flanking the common (Heinrich *et al.*, 2003b) mutation sites of *PDGFRA;* exons 10, 12, 14, and 18 (Table S1). No mutations of *PDGFRA* were found in any or our melanoma samples. Our samples contained a majority of tumor cells, which excludes the possibility that mutations were missed owing to an excess of stromal cells. In addition, all samples included in this analysis showed DNA copy number changes by CGH (Curtin *et al.*, 2005, 2006), which indicates that

Abbreviations: CSD, chronic sun damage; KIT, *v-kit Hardy-Zuckerman 4 feline sarcoma viral oncogene homolog;* NRAS, *neuroblastoma ras viral oncogene homolog;* PDGFRA, *platelet-derived growth factor α receptor*